Table 2
Summary of histopathological findings.

Compound	Toxicity class	Findings (renal tubule)	Low				Middle				High			
			4D	8D	15D	29D	4D	8D	15D	29D	4D	8D	15D	29D
Gentamicin sulphate	Tubular toxicant (direct/indirect)	Necrosis; degeneration; regeneration	0	0	0	1	0	0	0	1	1	1	1	1
Vancomycin hydrochloride		Degeneration; regeneration	0	0	0	0	0	0	0	2	1	1	1	1
2-Bromoethylamine hydrobromide		Regeneration	0	0	0	0	0	0	2	2	2	1	1	1
Phenylbutazone		Regeneration	0	0	0	0	0	0	0	0	1	1	1	1
Cyclosporine A		Degeneration; regeneration	0	0	0	0	0	1	1	1	1	1	1	1
Thioacetamide		Regeneration	0	0	0	0	0	0	1	0	1	1	1	1
K17		Necrosis; degeneration; regeneration	0	0	0	0	0	0	1	1	1	1	1	1
Triamterene		Regeneration	0	0	0	1	1	1	1	1	1	1	1	1
Allopurinol		Regeneration	0	0	0	0	1	1	1	1	1	1	1	1
Nitrofurantoin		Regeneration	0	0	0	0	1	1	0	0	1	1	1	0
Ethionine		Degeneration; regeneration	0	0	0	0	1	0	0	0	1	1	0	0
N-Phenylanthranilic acid		Regeneration	0	0	0	0	0	2	0	1	1	1	1	1
Cisplatin		Necrosis; degeneration; regeneration	0	0	0	0	0	0	1	1	1	1	1	1
Phenacetin		Regeneration	0	0	0	0	0	0	0	0	0	1	1	1
Puromycin aminonucleoside		Degeneration; regeneration	0	0	1	1	0	2	1	2	2	1		
Lomustine		Degeneration; regeneration	0	0	0	0	0	0	0	2	0	0	1	1
Cyclophosphamide		Regeneration	0	0	0	0	0	0	0	0	0	0	0	1
Carboplatin		Degeneration	0	0	0	0	0	0	0	0	0	0	0	1
Hexachlorobenzene		Regeneration	0	0	2	1	0	0	2	1	0	2	2	1
Captopril		Regeneration	0	0	0	0	0	0	0	1	0	0	0	1
Enalapril		Necrosis; regeneration	0	0	0	0	0	0	0	1	0	0	0	1
Indomethacin		Regeneration	0	0	0	0	0	0	0	0	0	2	1	
Doxorubicin hydrochloride		Necrosis; degeneration	0	0	0	0	0	0	0	0	0	0	0	1
Ethinyl estradiol	Potential tubular toxicant	Vacuolization	0	0	0	2	0	0	2	2	0	0	0	2
Monocrotaline		Anisonucleosis; vacuolization	0	0	0	0	0	0	0	2	0	2	2	
Acetaminophen		No-findings	0	0	0	0	0	0	0	0	0	0	0	0
Cephalothin sodium		Cytoplasmic granule	0	0	0	2	0	0	2	2	0	2	2	2
Bucetin		No-findings	0	0	0	0	0	0	0	0	0	0	0	0
Methyltestosterone		Hypertrophy	0	0	0	0	0	0	0	2	0	0	2	2
Rifampicin		Hyaline droplet; eosinophilic body	0	2	2	2	0	2	2	2	0	2	2	2
Imipramine hydrochloride	Hepatotoxicant (non-nephrotoxicant)	No-findings	0	0	0	0	0	0	0	0	0	0	0	0
Acetazolamide		No-findings	0	0	0	0	0	0	0	2	0	0	2	2
Caffeine		No-findings	0	0	0	0	0	0	0	0	0	0	0	0
Valproic acid		No-findings	0	0	0	0	0	0	0	0	0	0	0	0
Clofibrate		No-findings	0	0	0	0	0	0	0	0	0	0	0	0
Allyl alcohol		No-findings	0	0	0	0	0	0	0	0	0	0	0	0
Omeprazole		No-findings	0	0	0	0	0	0	0	0	0	0	0	0
Bromobenzene		No-findings	0	0	0	0	0	0	0	0	0	0	0	0
Ketoconazole		No-findings	0	0	0	0	0	0	0	0	0	0	0	0
Ciprofloxacin		No-findings	0	0	0	0	0	0	0	0	0	0	0	0
Erythromycin ethylsuccinate		No-findings	0	0	0	0	0	0	0	0	0	0	0	0

The absence or presence of renal tubular toxicity is indicated as 0 or 1 according to the following findings: necrosis, degeneration, and regeneration. Other histopathological findings, such as tubular vacuolation, hypertrophy, or intracytoplasmic hyaline droplet, are indicated as 2.

Table 3
Top 98 probes (92 genes) ranked by Intensity-Based Modified *T*-statistics.

Function	Rank	IBMT-value	Probe ID	Gene symbol	Gene title
Tissue remodeling	67	16.58035006	1368419_at	Cp	Ceruloplasmin
	53	17.38025275	1367655_at	Tmsb10	Thymosin, beta 10
	42	18.32495826	1368418_a_at	Cp	Ceruloplasmin
	35	18.71625959	1370511_at	Fgb	Fibrinogen, B beta polypeptide
	34	18.75582061	1370992_a_at	Fga	Fibrinogen, alpha polypeptide
	25	19.4777112	1368160_at	Igfbp1	Insulin-like growth factor binding protein 1
	23	20.04881639	1387011_at	Lcn2	Lipocalin 2
	5	23.34760498	1367581_a_at	Spp1	Secreted phosphoprotein 1
	4	24.99287138	1367784_a_at	Clu	Clusterin
	3	25.55598409	1368420_at	Cp	Ceruloplasmin
	2	27.31956855	1367712_at	Timp1	Tissue inhibitor of metallopeptidase 1
	1	32.37802533	1387965_at	Havcr1	Kidney injury molecule 1
Immune response/inflammatory response	95	15.48262595	1367850_at	Fcgr3	Fc receptor, IgG, low affinity III
	85	15.87707814	1367786_at	Psmb8	Proteosome (prosome, macropain) subunit, beta type 8
	82	15.95556487	1370892_at	C4-2	Complementcomponent4a
	57	17.08681361	1368490_at	Cd14	CD14 antigen
	49	17.46443444	1379889_at	Lamc2	Laminin, gamma 2
	36	18.6392526	1367794_at	A2m	Alpha-2-macroglobulin
	31	19.03400005	1374033_at	Psmb10	Proteasome (prosome, macropain) subunit, beta type 10
	26	19.3233011	1374119_at	Elf3	E74-like factor 3
	21	20.17343592	1368921_a_at	Cd44	CD44 antigen
	12	20.92295884	1367614_at	Anxa1	Annexin A1
	10	21.33883134	1379340_at	Lamc2	Laminin, gamma 2
	7	22.90158183	1387952_a_at	Cd44	CD44 antigen
Cell adhesion/proliferation/migration	68	−16.55652999	1368131_at	Capn6	Calpain 6
	89	−15.74490892	1372869_at	Gtpbp4	GTPbindingprotein4
	98	−15.44895153	1370144_at	Gtpbp4	GTPbindingprotein4
	59	16.9871558	1367574_at	Vim	Vimentin
	56	17.09543212	1388587_at	Ier3	Immediate early response 3
	50	17.46375719	1367914_at	Emp3	Epithelial membrane protein 3
	47	17.49603392	1370177_at	PVR	Poliovirus receptor
	45	17.78791131	1388802_at	Bex1	Brain expressed X-linked 1
	40	18.45920696	1368612_at	Itgb4	Integrin beta 4
	32	18.86869018	1375170_at	S100a11	S100 calcium binding protein A11 (calizzarin)
	20	20.20478694	1373421_at	Tgif	TG interacting factor
	19	20.41704079	1386879_at	Lgals3	Lectin, galactose binding, soluble 3
	18	20.63006692	1371785_at	Tnfrsf12a	Tumor necrosis factor receptor superfamily, member 12a
	16	20.67075085	1386890_at	S100a10	S100 calcium binding protein A10 (calpactin)
	14	20.72852871	1368187_at	Gpnmb	Glycoprotein (transmembrane) nmb
Membrane transport	70	−16.51359077	1388097_at	Cacng5	Calcium channel, voltage-dependent, gamma subunit 5
	94	15.49715091	1380909_at	–	Transcribed locus
	73	16.25219965	1368497_at	Abcc2	ATP-binding cassette, sub-family C (CFTR/MRP), member 2
	9	22.17460015	1368168_at	Slc34a2	Solute carrier family 34 (sodium phosphate), member 2
Metabolism	93	15.55951107	1370813_at	Gstm5	Glutathione S-transferase, mu 5
	87	15.78307408	1372691_at	Upp1	Uridine phosphorylase 1
	65	16.68114127	1374070_at	Gpx2	Glutathione peroxidase 2
	61	16.95386475	1374784_at	Prtfdc1_predicted	Phosphoribosyl transferase domain containing 1 (predicted)
	44	17.95904453	1370561_at	A3galt2	Alpha-1,3-galactosyltransferase 2 (isoglobotriaosylceramide synthase)
	39	18.4925478	1370445_at	Pspla1	Phosphatidylserine-specific phospholipase A1
	33	18.84407902	1387925_at	Asns	Asparagine synthetase
Apoptosis	84	15.89635722	1370113_at	Birc3	Baculoviral IAP repeat-containing 3
	75	16.23159672	1368308_at	Myc	Myelocytomatosis viral oncogene homolog (avian)
Signal transduction	38	−18.53296844	1370522_at	Gcgr	Glucagon receptor
	69	16.51817598	1390510_at	Ms4a6b	Membrane-spanning 4-domains, subfamily A, member 6B
Angiogenesis/fibrinolysis	30	19.03449106	1367584_at	Anxa2	Annexin A2
Blood coagulation	52	17.3941316	1368052_at	Tspan8	Tetraspanin 8
Cell–cell communication	81	16.08958043	1388547_at	Cldn4	Claudin 4

Table 3 (*Continued*)

Function	Rank	IBMT-value	Probe ID	Gene symbol	Gene title
Detection of temperature stimuli	15	20.67755397	1367768_at	Lxn	Latexin
DNA replication initiation	97	15.47163164	1372406_at	LOC367976	Minichromosomemaintenancedeficient3 (S.cerevisiae)(predicted)
Endocytosis	80	16.0961982	1392648_at	Mrc1_predicted	Mannose receptor, C type 1 (predicted)
Kidney development	78	16.13533388	1368223_at	Adamts1	A disintegrin-like and metallopeptidse (reprolysin type) with thrombospondin type 1 motif, 1
Microtubule-based process	71	16.33428851	1387892_at	Tubb5	Tubulin, beta 5
miRNA-mediated gene silencing	88	15.75295308	1371583_at	Rbm3	RNA binding motif protein 3
rRNA processing	24	19.83460167	1373499_at	Gas5	Growth arrest specific 5
Stress fiber formation	58	17.05771651	1373286_at	Fblim1	Filamin binding LIM protein 1
Structural constituent of cytoskeleton	86	15.805369	1370288_a_at	Tpm1	Tropomyosin 1, alpha
	92	15.57704782	1382590_at	RGD1563347_predicted	Similar to RIKEN cDNA 2310015N21 (predicted)
	79	16.12099714	1376877_at	Cdcp1_predicted	CUB domain containing protein 1 (predicted)
	77	16.15247506	1368207_at	Fxyd5	FXYD domain-containing ion transport regulator 5
	62	16.9053337	1390226_at	RGD1562552_predicted	Similar to hypothetical protein LOC340061 (predicted)
	55	17.14203525	1389659_at	RGD1565540_predicted	Similar to ctla-2-beta protein (141 AA) (predicted)
	51	17.42187372	1393240_at	Efemp2	EGF-containing fibulin-like extracellular matrix protein 2
	29	19.0788577	1393643_at	Rcn1_predicted	Reticulocalbin 1 (predicted)
	28	19.09794144	1383401_at	LOC500040	Similar to Testis derived transcript
	13	−20.76507248	1390847_at	Tmem86a_predicted	Transmembrane protein 86A (predicted)
ESTs	17	−20.6670163	1373309_at	Tmem86a_predicted	Transmembrane protein 86A (predicted)
	96	−15.4719928	1374167_at	LOC361399	Similar to autoantigen
	90	15.72117787	1388340_at	Ns5atp9	NS5A (hepatitis C virus) transactivated protein 9
	83	15.92546837	1375224_at	Phlda3	Pleckstrin homology-like domain, family A, member 3
	72	16.3017568	1373035_at	–	–
	66	16.62012551	1390109_at	–	–
	64	16.80319643	1373908_at	–	–
	60	16.96481687	1371782_at	Nipsnap3a	Nipsnap homolog 3A (C. elegans)
	54	17.20576139	1373504_at	Glipr1	GLI pathogenesis-related 1 (glioma)
	43	17.9919912	1379957_at	Slfn8	Schlafen 8
	27	19.2586905	1388900_at	RGD1566118_predicted	RGD1566118 (predicted)
	22	20.17177219	1390839_at	Pqlc3	PQ loop repeat containing 3
	41	−18.40682675	1372911_at	–	Transcribed locus
	46	−17.76332084	1376913_at	–	Transcribed locus
	91	−15.59722933	1378292_at	–	Transcribed locus
	76	16.20156037	1385190_at	–	Transcribed locus
	74	16.23557955	1377994_at	–	Transcribed locus
	63	16.82551948	1397769_at	–	Transcribed locus
	48	17.48169748	1393252_at	–	Transcribed locus
	37	18.59863244	1376109_at	–	Transcribed locus
	11	20.9365083	1377092_at	–	Transcribed locus
	8	22.29041324	1391106_at	–	Transcribed locus
	6	23.16631514	1390659_at	–	Transcribed locus

values by the variance of the log-ratio value of the control samples calculated for each arbitrary range of the expression values. Then, the expression values of the control samples were pooled for each compound and time point ($n=3$). Among the 92 genes, 83 genes were significantly up-regulated, and 9 genes were down-regulated in most of the positive samples (Fig. 1, Table 3). Most of the genes involved in tissue remodeling, the immune/inflammatory response, cell adhesion/proliferation/migration, and metabolism were up-regulated. Several up-regulated genes were also involved in membrane transport, signal transduction, apoptosis, and some of the other genes that were probably related to reconstruction of the kidney tissues (e.g., structural constituent of cytoskeleton). In particular, genes involved in tissue remodeling and the immune/inflammatory response had many well-known biomarker candidates for renal tubular injury, as described by Wang et al. (2008) (8/10 and 2/10, respectively). Down-regulated genes participated in cell adhesion/proliferation/migration, membrane transport, and signal transduction.

Most of the 10 genes that participated in tissue remodeling were strongly up-regulated (Z-score > 2.5) in most of the positive samples (Fig. 1a). On day 4, a lot of genes already had been up-regulated after treatment with vancomycin hydrochloride, 2-bromoethylamine hydrobromide, phenylbutazone, cyclosporine A, thioacetamide, K17, triamterene, allopurinol, ethionine, *N*-phenylanthranilic acid, cisplatin, phenacetin, captopril, enalapril, and indomethacin. With the exceptions of 2-bromoethylamine

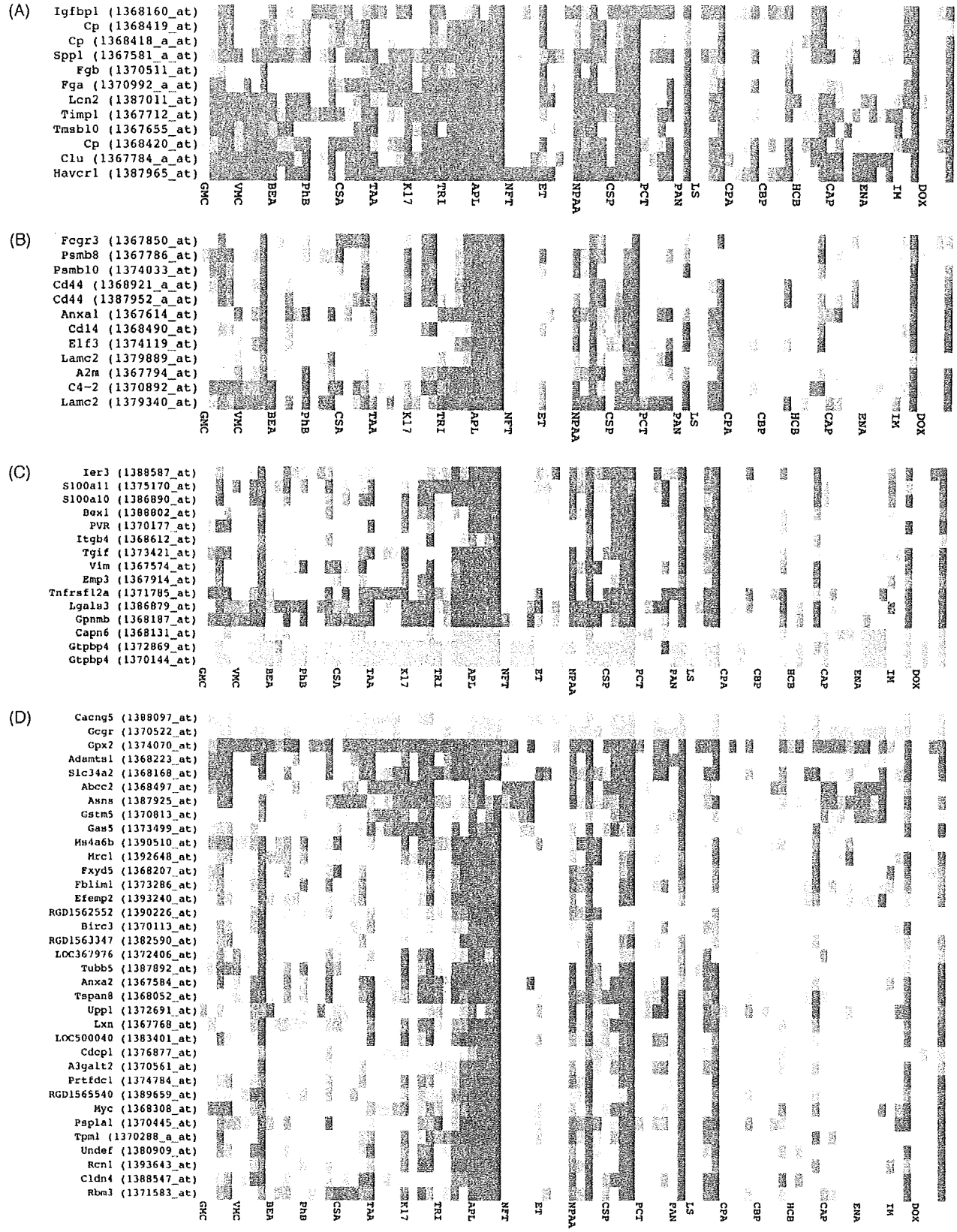

Fig. 1. The gene expression profile of the feature genes. Rows – genes, columns – sample groups. Each color represents the *Z*-score of the log-ratio to the mean expression value of the corresponding control samples (same compound and time point). Up-regulated genes (*Z*-score ≥ 2.5) are represented by red colors, and down-regulated genes (*Z*-score ≤ −2.5) are represented by blue colors. Each sample group is labeled with the compound abbreviation on day 4. The columns of each compound are ordered in time (from day 4 to day 29). (a) Tissue remodeling, (b) immune/inflammatory response, (c) cell adhesion/proliferation/migration, and (d) the others (membrane transport, metabolism, signal transduction, apoptosis). (For interpretation of the references to color in this figure legend, the reader is referred to the web version of the article.)

hydrobromide, phenacetin, captopril, enalapril, and indomethacin, histopathological findings had been observed in the animals treated with the above 10 compounds on day 4 (Table 2). In the case of 2-bromoethylamine hydrobromide, phenacetin, captopril, enalapril, and indomethacin, the histopathological findings were observed after day 8; therefore, these feature genes had been up-regulated before histopathological changes (in 2-bromoethylamine hydrobromide, slight dilatation of the cortex was observed in 1 of 5 animals). The animals treated with gentamicin sulphate and nitrofurantoin had histopathological findings on day 4, but predominant up-regulation of tissue remodeling-related genes was not observed. Puromycin aminonucleoside-, lomustine-, cyclophosphamide-, carboplatin-, hexachlorobenzene-, and doxorubicin hydrochloride-treated samples had neither histopathological findings nor induction of tissue remodeling-related genes on day 4 (in puromycin aminonucleoside, a slight hyaline droplet in the cortex was observed in 1 of 5 animals). Although, except for puromycin aminonucleoside, predominant up-regulation of the feature genes related to tissue remodeling was observed before the histopathological changes. On the other hand, nitrofurantoin-treated animals did not exhibit predominant induction of the genes at any of the time points examined. Ethionine-treated animals had histopathological findings on day 4, but recovered from pathological status on day 15, which is the same as nitrofurantoin-treated animals. In contrast to nitrofurantoin, predominant up-regulation was found in the animals treated with ethionine on days 4, 8, and 15, but the up-regulated genes gradually decreased in a time-dependent manner. While some of the feature genes were also up-regulated in some of the negative samples, the extent of up-regulation of these genes was weak compared to those in the high-dose groups of the positive compounds.

Although the immune/inflammatory response-related genes were not universally induced in the positive samples as compared to tissue-remodeling related genes, predominant up-regulation was observed in most of the positive compounds (Fig. 1b). The animals treated with 2-bromoethylamine hydrobromide exhibited predominant up-regulation on day 4, and some of the genes were up-regulated in phenacetin, captopril, and indomethacin before histopathological changes in a similar manner seen in tissue remodeling. nitrofurantoin- and enalapril-treated animals did not exhibit predominant up-regulation of the genes at any of the time points. In the case of thioacetamide and ethionine, predominant up-regulation was only found on day 4, despite the histopathological findings observed after day 4.

Among the 14 cell adhesion/proliferation/migration-related genes, 2 genes were predominantly down-regulated, and 12 genes were predominantly up-regulated in most of the positive compounds (Fig. 1c). In 2-bromoethylamine hydrobromide, cyclophosphamide, hexachlorobenzene, captopril, enalapril, indomethacin, and doxorubicin hydrochloride, some of the feature genes were induced before histopathological changes. In nitrofurantoin and ethionine, some of the feature genes were induced after histopathological findings disappeared. *Gtpbp4* (*GTP-binding protein 4*) was down-regulated in most of the positive compounds and up-regulated in a lot of negative compounds.

Genes in other functional categories were also induced (Fig. 1d). Seven genes related to metabolism were up-regulated. Among them, *Gpx2* (*glutathione peroxidase 2*) was not only up-regulated in most of the positive compounds, but also in some of the negative compounds. The other xenobiotic metabolic enzyme, *Gstm5* (*glutathione S-transferase, mu 5*), was not induced in some of the positive compounds. Most of the genes related to metabolism (probably involved in secondary compensatory mechanism of cell toxicity) were strongly up-regulated in the positive compounds that exhibited histopathological findings throughout chronic administration. On the other hand, *Asns* (*asparagines synthetase*) was also induced in nitrofurantoin, thioacetamide, captopril, and enalapril, which exhibited histopathological findings only at the beginning or after long-term administration. *Abcc2* (*ATP-binding cassette, sub-family C, member 2*), which act as a multi-drug transporter, was also up-regulated in nitrofurantoin, thioacetamide, captopril, and enalapril. But, these two genes were also predominantly induced in the negative compounds (clofibrate or omeprazole). In summary, the same as for the other functional categories, the late-onset compounds (e.g., cyclophosphamide, captopril, enalapril) did not tend to predominantly induce the genes of the above functional categories at the early stage of administration, and the recovered compounds (e.g., 2-bromoethylamine hydrobromide, nitrofurantoin, and ethionine) did not induce these genes at the late stage. It seems that the expression profiles of the feature genes were not necessarily correlated to the severity of the histopathological findings at the time point; rather, they were correlated to the time-dependent profile of histopathological changes.

3.2.3. *Prediction of the external test compounds*

Middle-dose groups of all 41 compounds and high-dose groups of 10 compounds (and also high-dose groups of the remaining 31 compounds at the time points without histopathological findings), which had not been used as the training set, were used as the test set for further external validation of the classifier. As a result, 11 of 14 (78.5%) compounds of the middle-dose groups with histological lesions were correctly classified into the positive group of renal tubular injury, when we used SVM positive probability of 0.5 as the threshold (Table 4). Among them, captopril and enalapril exhibited predominant induction of tissue remodeling-related genes and some of the other genes (e.g., *Gtpbp4*, *Gpx2*, *Abcc2*) and were predicted as positive before any signs of tubular damage had occurred. The middle-dose group of LS on day 29 was classified into the positive group without the presence of tubular damage (the high-dose groups of the compound exhibited tubular damage). On the other hand, allopurinol, nitrofurantoin, and *N*-phenylanthranilic acid, which had histopathological findings at the middle-dose groups, were classified into the negative group. Although, in the case of allopurinol and *N*-phenylanthranilic acid, many feature genes were induced and had comparatively higher SVM probabilities.

Among 23 tubular toxicants, the high-dose groups of 11 compounds exhibited late onset of the histopathological findings. Seven of these 11 compounds (63.6%) were predicted as positive before histopathological changes (2-bromoethylamine hydrobromide, phenacetin, carboplatin, hexachlorobenzene, captopril, enalapril, and indomethacin). We also calculated SVM probabilities for the high- and middle-dose groups of 10 potential tubular toxicants and predicted 5 of the 10 compounds as positive (ethinyl estradiol, monocrotaline, acetaminophen, imipramine hydrochloride, and acetazolamide). In most of the compounds predicted as positive without histopathological findings at the early stage of drug-administration or at the lower dosage, a lot of feature genes of most of the functional categories had been already induced (especially tissue remodeling).

4. Discussion

In the present study, we identified 98 genomic biomarker candidates (92 genes) and successfully constructed a highly accurate classifier for the concurrent diagnosis of renal tubular injury using diverse groups of nephrotoxicants and hepatotoxicants. We first compared different types of gene selection and classification algorithms to select the best analytical methods (SVM+IBMT; Supplementary figures). Then, the external test sets were randomly generated 100 times to validate the classifiers. Most of the previous reports that executed a toxicogenomics analysis of renal tubular

Table 4
Histopathological findings and the result of the prediction of the further external test set.

Compound	Toxicity class	SVM positive probability											
		Low				Middle				High			
		4D	8D	15D	29D	4D	8D	15D	29D	4D	8D	15D	29D
Gentamicin sulphate		0.007	0.017	0.144	0.088	0.012	0.067	0.391	1.000	0.121	1.000	1.000	1.000
Vancomycin hydrochloride		0.002	0.003	0.006	0.008	0.004	0.003	0.006	0.036	0.929	0.901	1.000	1.000
2-Bromoethylamine hydrobromide		0.024	0.015	0.020	0.010	0.039	0.103	0.024	0.023	0.996	0.853	0.996	0.879
Phenylbutazone		0.054	0.029	0.066	0.015	0.064	0.062	0.115	0.020	0.996	0.524	0.872	1.000
Cyclosporine A		0.015	0.045	0.053	0.035	0.129	0.887	0.857	0.990	0.992	1.000	1.000	1.000
Thioacetamide		0.057	0.030	0.014	0.027	0.348	0.176	0.680	0.848	1.000	0.992	1.000	1.000
K17		0.006	0.308	0.148	0.035	0.320	0.107	0.996	0.992	1.000	1.000	1.000	1.000
Triamterene		0.044	0.016	0.006	0.013	0.581	0.046	0.947	0.721	1.000	0.991	1.000	1.000
Allopurinol		0.005	0.003	0.018	0.050	0.068	0.417	0.025	0.244	1.000	1.000	1.000	1.000
Nitrofurantoin		0.040	0.003	0.013	0.018	0.018	0.005	0.021	0.064	0.328	0.179	0.192	0.906
Ethionine		0.095	0.040	0.038	0.018	0.819	0.030	0.046	0.028	0.983	0.460	0.164	0.040
N-Phenylanthranilic acid	Tubular toxicant (direct/indirect)	0.076	0.030	0.040	0.035	0.032	0.164	0.128	0.400	1.000	1.000	1.000	1.000
Cisplatin		0.013	0.097	0.010	0.109	0.044	0.433	0.910	0.996	0.966	1.000	1.000	1.000
Phenacetin		0.005	0.006	0.027	0.004	0.008	0.011	0.034	0.012	0.688	0.931	1.000	1.000
Puromycin aminonucleoside		0.007	0.028	0.028	0.098	0.015	0.024	1.000	1.000	0.418	1.000	NA	NA
Lomustine		0.012	0.048	0.101	0.011	0.015	0.022	0.287	0.721	0.007	0.155	1.000	1.000
Cyclophosphamide		0.009	0.061	0.032	0.008	0.044	0.024	0.009	0.014	0.044	0.132	0.152	0.919
Carboplatin		0.006	0.014	0.020	0.009	0.007	0.046	0.116	0.277	0.046	0.331	0.600	1.000
Hexachlorobenzene		0.010	0.011	0.098	0.536	0.058	0.174	0.121	1.000	0.027	0.300	0.743	1.000
Captopril		0.004	0.015	0.063	0.031	0.028	0.552	0.639	0.953	0.970	0.967	0.910	0.959
Enalapril		0.039	0.343	0.066	0.064	0.058	0.423	0.920	0.674	0.307	0.958	0.574	0.972
Indomethacin		0.069	0.004	0.004	0.011	0.053	0.013	0.029	0.061	0.661	0.910	1.000	NA
Doxorubicin hydrochloride		0.008	0.015	0.013	0.025	0.010	0.022	0.009	0.018	0.004	0.021	0.025	1.000
Ethinyl estradiol		0.048	0.069	0.108	0.138	0.252	0.079	0.612	0.605	0.640	0.191	0.642	0.668
Monocrotaline		0.004	0.018	0.019	0.051	0.011	0.116	0.218	0.864	0.044	0.986	1.000	NA
Acetaminophen		0.026	0.039	0.011	0.042	0.021	0.185	0.019	0.365	0.458	0.143	0.932	0.981
Cephalothin sodium		0.011	0.013	0.009	0.008	0.109	0.008	0.006	0.042	0.143	0.047	0.060	0.120
Bucetin	Potential tubular toxicant	0.005	0.007	0.024	0.023	0.019	0.016	0.003	0.035	0.007	0.030	0.119	0.038
Methyltestosterone		0.024	0.011	0.001	0.005	0.003	0.004	0.006	0.011	0.005	0.030	0.081	0.170
Rifampicin		0.014	0.017	0.004	0.008	0.007	0.024	0.010	0.090	0.224	0.052	0.060	0.317
Imipramine Hydrochloride		0.016	0.009	0.027	0.018	0.022	0.012	0.068	0.002	0.022	0.104	0.547	0.118
Acetazolamide		0.049	0.034	0.017	0.011	0.049	0.586	0.098	0.035	0.039	0.209	0.192	0.159
Caffeine		0.007	0.008	0.011	0.005	0.003	0.011	0.006	0.014	0.047	0.019	0.016	0.021
Valproic acid		0.002	0.003	0.026	0.006	0.007	0.011	0.029	0.008	0.020	0.041	0.056	0.016
Clofibrate		0.034	0.032	0.007	0.006	0.026	0.017	0.007	0.024	0.158	0.022	0.077	0.072
Allyl alcohol		0.004	0.010	0.015	0.008	0.004	0.017	0.006	0.004	0.003	0.031	0.006	0.013
Omeprazole	Hepatotoxicant	0.007	0.015	0.036	0.032	0.032	0.244	0.079	0.008	0.011	0.036	0.136	0.052
Bromobenzene		0.006	0.004	0.005	0.007	0.019	0.007	0.039	0.009	0.005	0.007	0.039	0.026
Ketoconazole		0.004	0.004	0.012	0.003	0.007	0.004	0.011	0.007	0.022	0.009	0.015	0.010
Ciprofloxacin		0.008	0.009	0.007	0.026	0.007	0.015	0.009	0.012	0.010	0.003	0.007	0.020
Erythromycin ethylsuccinate		0.006	0.013	0.025	0.020	0.009	0.018	0.045	0.083	0.054	0.025	0.073	0.113

injury did not use an external test set or used only one external test set. These approaches were not statistically robust or biologically appropriate, because the prediction accuracy was possibly differentiated and deviated depending on how the whole dataset was split into the external test set and the training set. Because we used a variety of compounds, it was especially important to randomize the external test set for our analysis to avoid statistical deviations. Furthermore, we validated their prediction accuracies using middle-dose groups of all 41 compounds and the high-dose groups of 23 compounds that were not used in the training of the classifier. The classifier constructed by the genomic signatures exhibited a higher sensitivity than the histopathological findings in detecting renal tubular damage at lower doses and at earlier time points (Table 4). Our large-scale, high-quality toxicogenomics database and algorithms for gene selection and classification have higher statistical power than any of the previous studies and are very useful for robust biomarker selection and the prediction of drug-induced toxicities.

The feature genes that could be biomarker candidates for drug-induced renal tubular injury include several well-known biomarker candidate genes, such as *Kim1*, *Cp*, *Clu*, *Timp1*, and *Spp1*. We also identified several genes that were not frequently reported in previous studies but are included in functional categories thought to be mechanistically related to tubular toxicity, and the expression levels of these genes were correlated to the severity of the histopathological findings (Fig. 1). Wang et al. (2008) recently conducted a literature survey to collect tubular injury biomarkers that were described in multiple published studies, and they validated these biomarkers by using RT-PCR. Our gene list contains 11 of 24 validated genes (Table 3). Among the 11 genes, 8 genes are involved in tissue remodeling, and 2 genes are involved in the immune/inflammatory response. All of tissue remodeling and immune/inflammatory response-related genes were up-regulated, as described in the previous studies. These genes are thought to be related to secondary compensatory mechanisms of renal tubular injury (Huang et al., 2001). Eight of 10 tissue remodeling-related genes were consistent with the genes reported by Wang et al., and most of these genes were strongly up-regulated in most of the positive samples. The genes that participated in these two functional categories were strongly suggested as genomic biomarker candidates for drug-induced renal tubular injury.

We found that the up-regulation of tissue remodeling and immune/inflammatory-related genes was most prominently induced and roughly consistent with or induced earlier than the histopathological findings (Fig. 1a and b). Up-regulated genes also participated in metabolism, cell adhesion/proliferation/migration, apoptosis, membrane transport, and signal transduction (Fig. 1c and d). Two xenobiotics metabolism-related genes (*Gpx2*, *Gstm5*) were up-regulated, probably in response to oxidative stress (Rokushima et al., 2008). *Asns* (*Asparagine synthetase*) is crucial for asparagine synthesis and may be important for progression through the G1 phase of the cell cycle (Hutson and Kilberg, 1994). *A3galt2* (*alpha-1,3-galactosyltransferase 2*) is involved in the synthesis of the isoglobo-series of glycosphingolipids, which are suggested to be involved in apoptosis. *Pspla1* (*phosphatidylserine-specific phospholipase A1*) stimulates histamine release and, therefore, may be involved in the inflammatory response (Hosono et al., 2001). Some membrane transporters including the multidrug transporter were up-regulated and probably are commonly induced by the toxicities of the diverse class of nephrotoxicants. Up-regulated genes related to cell adhesion/proliferation/migration and apoptosis also would be related to secondary compensatory mechanisms, the same as for genes related to tissue remodeling and the immune/inflammatory response. Several of these genes have been reported as genomic biomarkers of renal tubular injury.

Down-regulated genes participated in cell adhesion/proliferation/migration, membrane transport, and signal transduction (Fig. 1c and d). The down-regulation may be a response to drug-induced toxicity or an adverse effect and may serve to maintain a low cellular energy status to minimize further damage (Safirstein et al., 1990). Down-regulation occurs during the acute phase of tubular damage induced by nephrotoxicants and acute ischemic renal injury (Amin et al., 2004; Hu et al., 2000; Huang et al., 2001). Representative down-regulated genes observed in our analysis were *Cacng5* (*calcium channel, voltage-dependent, gamma subunit 5*) and *Gcgr* (*glucagons receptor*). Calcium channels transport calcium ions in cell cytoplasm to the outside and maintain their gradient of concentration. Down-regulation of *Cacng5* may be a consequence of lower energy status or the perturbation of calcium homeostasis. Glucagons are peptide hormones that suppress glycolysis and accelerate gluconeogenesis. Therefore, down-regulation of *Gcgr* probably suppresses gluconeogenesis. Our results show that the down-regulation of energy-consuming processes is also observed in chronic renal tubular injury.

In summary, our results support previous studies that described correlations between well-known biomarker candidate genes or their functional categories and renal tubular injury. We used not only typical compounds that cause renal tubular injury but also a lot of compounds that have diverse effects and different patterns of histopathological changes with multiple time points and dosages. Our results suggest that well-known biomarkers and their functional categories for renal tubular injury are also induced by a wide variety of nephrotoxicants. On the other hand, we also found inconsistent and novel analytical results and heterogeneities between compounds that have different patterns of histopathological changes. It is thought that our gene list preferentially contains genes concerning secondary compensatory mechanisms rather than drug toxicity because of the diversity of the compounds used in our analysis. The feature genes were highly and commonly induced in the compounds, thus, the feature genes are highly statistically reliable and useful as genomic biomarkers during the drug-development process. On the other hand, it is also important to investigate the differences in gene expression profiles corresponding to the toxicity between diverse classes of compounds.

We used middle-dose groups and high-dose groups, which had not been used in the training set, as a further external test set for our classifier constructed from 98 top-ranked genomic biomarkers. Eleven of 14 compounds (78.5%) with histopathological findings at middle-dose groups were correctly classified as positive (Table 4). Also, some of these compounds were predicted as positive at the time points before the emergence of the tubular injury. These results indicate that genomic biomarkers are more sensitive than histopathological findings. On the other hand, although the middle-dose groups of allopurinol, nitrofurantoin, and *N*-phenylanthranilic acid exhibited histopathological findings, these compounds were predicted as negative. In the case of high- and middle-dose nitrofurantoin, renal tubular necrosis had been already observed within 24 h after administration (data not shown) and recovered after day 15. We found that most of our 98 genomic biomarker candidates were not significantly induced at the middle-dose groups of nitrofurantoin (Supplementary figure). Instead, the high-dose groups of nitrofurantoin exhibited gene expression changes in some of the 92 genes, and were predicted as positive (day 29). Therefore, it is thought that the gene expression profiles of middle-dose nitrofurantoin may reflect the recovery from tubular injury, even though the histopathological findings were still observed. In the case of *N*-phenylanthranilic acid, 3 of 5 animals sacrificed on day 29 did not exhibit any histopathological changes. In the case of allopurinol and *N*-phenylanthranilic

acid, many feature genes were induced and had comparatively higher SVM probabilities. These samples should be included in the training set to construct better classifiers, or heterogeneity may exist.

We also used the high-dose groups of 10 potential tubular toxicants as the test set. These compounds exhibited no histopathological findings of renal tubules (necrosis, degeneration, and regeneration), but the induction of renal tubular injury and/or other nephrotoxicities have been described in previous reports. Five of the 10 compounds (ethinyl estradiol, monocrotaline, acetaminophen, imipramine hydrochloride, and acetazolamide) were predicted as renal tubular injury positive. Monocrotaline- and ethinyl estradiol-treated animals had no tubular injury, and these compounds have not been reported as tubular toxicants. But, these compounds had anisonucleosis and/or vacuolization at cortex/proximal tubules. Acetaminophen was reported as a tubular toxicant. Therefore, it is reasonable that these three compounds were predicted as renal tubular toxicants. Imipramine hydrochloride- and acetazolamide-treated animals had no tubular injury, and these compounds have not been reported as tubular toxicants; thus, these may be false positives. However, in the high-dose group of imipramine hydrochloride on day 15, many of the feature genes, such as *Cp*, *Igfbp1*, *Fcgr3*, and *Cd14*, were induced. In the middle-dose group of acetazolamide on day 8, most of the genes related to tissue remodeling were strongly up-regulated, including *Kim1*, *Clu*, *Timp1*, *Cp*, and *Spp1*. Although these changes may reflect the early onset of nephrotoxicity, the possibility of false positives cannot be completely excluded.

The classifier constructed from multiple feature genes had much better prediction accuracy than classifiers constructed from any of the single or multiple well-known genomic biomarkers described above, histopathological findings, and any previous study (Fig. 3, Supplementary figure). Toxicogenomics and the large-scale database would be very useful in drug discovery and also helpful in risk estimation of nephrotoxicity. But, our analytical results suggest that there still exists unknown heterogeneity of gene expression between compounds that have different patterns of histopathological changes (times, severity, type of histopathological findings, etc.), even though the gene expression changes are concurrent with the histopathological findings. Also, further work is needed to adapt these genes into a toxicity screen by validating their reversibility and developing robust and convenient assays. We are now preparing experimental validation of our genomic biomarkers for concurrent diagnosis and gene expression analysis of further compounds. Accumulation of knowledge about various types of toxicities is very useful and important not only to identify specific biomarkers for an arbitrary toxicity, but also to understand mechanisms of drug-inducible toxicities.

Conflict of interest statement

The authors declare that there are no conflicts of interest.

Acknowledgements

This work was supported in part by the grants from Ministry of Health, Labour and Welfare of Japan, H14-001-Toxico and H19-001-Toxico.

Appendix A. Supplementary data

Supplementary data associated with this article can be found, in the online version, at doi:10.1016/j.tox.2009.09.003.

References

Amin, R.P., Vickers, A.E., Sistare, F., Thompson, K.L., Roman, R.J., Lawton, M., Kramer, J., Hamadeh, H.K., Collins, J., Grissom, S., Bennett, L., Tucker, C.J., Wild, S., Kind, C., Oreffo, V., Davis 2nd, J.W., Curtiss, S., Naciff, J.M., Cunningham, M., Tennant, R., Stevens, J., Car, B., Bertram, T.A., Afshari, C.A., 2004. Identification of putative gene based markers of renal toxicity. Environ. Health Perspect. 112, 465–479.

Battershill, J.M., 2005. Toxicogenomics: regulatory perspective on current position. Hum. Exp. Toxicol. 24, 35–40.

Fielden, M.R., Eynon, B.P., Natsoulis, G., Jarnagin, K., Banas, D., Kolaja, K.L., 2005. A gene expression signature that predicts the future onset of drug-induced renal tubular toxicity. Toxicol. Pathol. 33, 675–683.

Guyon, I., Weston, J., Barnhill, S., Vapnik, V., 2002. Gene selection for cancer classification using support vector machines. Mach. Learn. 46, 389–422.

Heinloth, A.N., Irwin, R.D., Boorman, G.A., Nettesheim, P., Fannin, R.D., Sieber, S.O., Snell, M.L., Tucker, C.J., Li, L., Travlos, G.S., Vansant, G., Blackshear, P.E., Tennant, R.W., Cunningham, M.L., Paules, R.S., 2004. Gene expression profiling of rat livers reveals indicators of potential adverse effects. Toxicol. Sci. 80, 193–202.

Hosono, H., Aoki, J., Nagai, Y., Bandoh, K., Ishida, M., Taguchi, R., Arai, H., Inoue, K., 2001. Phosphatidylserine-specific phospholipase A1 stimulates histamine release from rat peritoneal mast cells through production of 2-acyl-1-lysophosphatidylserine. J. Biol. Chem. 276, 29664–29670.

Hu, E., Chen, Z., Fredrickson, T., Gellai, M., Jugus, M., Contino, L., Spurr, N., Sims, M., Halsey, W., Van Horn, S., Mao, J., Sathe, G., Brooks, D., 2000. Identification of a novel kidney-specific gene downregulated in acute ischemic renal failure. Am. J. Physiol. Renal Physiol. 279, F426–F439.

Huang, Q., Dunn 2nd, R.D., Jayadev, S., DiSorbo, O., Pack, F.D., Farr, S.B., Stoll, R.E., Blanchard, K.T., 2001. Assessment of cisplatin-induced nephrotoxicity by microarray technology. Toxicol. Sci. 63, 196–207.

Hutson, R.G., Kilberg, M.S., 1994. Cloning of rat asparagine synthetase and specificity of the amino acid-dependent control of its mRNA content. Biochem. J. 304, 745–750.

Irwin, R.D., Boorman, G.A., Cunningham, M.L., Heinloth, A.N., Malarkey, D.E., Paules, R.S., 2004. Application of toxicogenomics to toxicology: basic concepts in the analysis of microarray data. Toxicol. Pathol. 32 (Suppl. 1), 72–83.

Jiang, Y., Gerhold, D.L., Holder, D.J., Figueroa, D.J., Bailey, W.J., Guan, P., Skopek, T.R., Sistare, F.D., Sina, J.F., 2007. Diagnosis of drug-induced renal tubular toxicity using global gene expression profiles. J. Transl. Med. 5, 47.

Perazella, M.A., 2005. Drug-induced nephropathy: an update. Expert Opin. Drug Saf. 4, 689–706.

Ransohoff, D.F., 2004. Rules of evidence for cancer molecular-marker discovery and validation. Nat. Rev. Cancer 4, 309–314.

Rokushima, M., Fujisawa, K., Furukawa, N., Itoh, F., Yanagimoto, T., Fukushima, R., Araki, A., Okada, M., Torii, M., Kato, I., Ishizaki, J., Omi, K., 2008. Transcriptomic analysis of nephrotoxicity induced by cephaloridine, a representative cephalosporin antibiotic. Chem. Res. Toxicol. 21, 1186–1196.

Safirstein, R., Price, P.M., Saggi, S.J., Harris, R.C., 1990. Changes in gene expression after temporary renal ischemia. Kidney Int. 37, 1515–1521.

Sartor, M.A., Tomlinson, C.R., Wesselkamper, S.C., Sivaganesan, S., Leikauf, G.D., Medvedovic, M., 2006. Intensity-based hierarchical Bayes method improves testing for differentially expressed genes in microarray experiments. BMC Bioinformatics 7, 538.

Searfoss, G.H., Ryan, T.P., Jolly, R.A., 2005. The role of transcriptome analysis in pre-clinical toxicology. Curr. Mol. Med. 5, 53–64.

Somorjai, R.L., Dolenko, B., Baumgartner, R., 2003. Class prediction and discovery using gene microarray and proteomics mass spectroscopy data: curses, caveats, cautions. Bioinformatics 19, 1484–1491.

Tibshirani, R., Hastie, T., Narasimhan, B., Chu, G., 2002. Diagnosis of multiple cancer types by shrunken centroids of gene expression. Proc. Natl. Acad. Sci. U.S.A. 99, 6567–6572.

Thukral, S.K., Nordone, P.J., Hu, R., Sullivan, L., Galambos, E., Fitzpatrick, V.D., Healy, L., Bass, M.B., Cosenza, M.E., Afshari, C.A., 2005. Prediction of nephrotoxicant action and identification of candidate toxicity-related biomarkers. Toxicol. Pathol. 33, 343–355.

Urushidani, T., Nagao, T., 2005. Toxicogenomics: the Japanese initiative. In: Borlak, J. (Ed.), Handbook of Toxicogenomics-Strategies and Applications. Wiley-VCH, Weinheim, pp. 623–631.

Vapkin, V., 1995. The Nature of Statistical Learning Theory. Springer-Verlag, New York, Inc.

Wang, E.J., Snyder, R.D., Fielden, M.R., Smith, R.J., Gu, Y.Z., 2008. Validation of putative genomic biomarkers of nephrotoxicity in rats. Toxicology 246, 91–100.

The Journal of Toxicological Sciences (J. Toxicol. Sci.)
Vol.34, Special Issue 1, SP189-SP197, 2009

Morphological characterization of the ovary under normal cycling in rats and its viewpoints of ovarian toxicity detection

Midori Yoshida[1], Atsushi Sanbuissyo[2], Shigeru Hisada[3], Michihito Takahashi[4], Yasuo Ohno[5] and Akiyoshi Nishikawa[1]

[1]Division of Pathology, Biology Safety Research Center, National Institute of Health Sciences, 1-18-1 Kamiyoga, Setagaya-ku, Tokyo 158-8501, Japan
[2]Medical Safety Research Laboratories, R & D Division, Daiichi-Sankyo Co., Ltd., 717 Horikoshi, Fukuroi, Shizuoka 437-0065, Japan
[3]Safety Research Department, Aska Pharmaceutical Co. Ltd., 1604 Shimosakunobe, Taktsu-ku, Kawasaki 213-8522, Japan
[4]Pathology Peer Review Center, 3-45-11 Uehara, Shibuya-ku, Tokyo 151-0064, Japan
[5]National Institute of Health Sciences, 1-18-1 Kamiyoga, Setagaya-ku, Tokyo 158-8501, Japan

(Received December 10, 2008)

ABSTRACT — Identification of ovarian toxicity is very important for safety assessment of drugs and other environmental chemicals. The detection of interference with ovarian function is very hard without a thorough understanding of the normal ovarian morphology based on reproductive physiology. The focus of the present study was therefore a practical analysis in each stage of the estrous cycles using ovaries obtained from 143 rats demonstrating normal cycling. Transversely dissected maximum areas in the ovaries were examined microscopically for the two major features, follicles and corpora lutea (CL). Classification of growing follicles was in reference to Pedersen and Peters (1968), and functionally divided into follicular stimulating hormone (FSH)-independent and dependent categories. The former, small and medium-sized follicles, respectively primordial/primary and preantral follicles, could be readily detected by immunohistochemical staining for proliferating cell nuclear antigen (PCNA). The large antral and Graafian follicles and large sized atretic follicles showed sequential changes depending on the estrous cycle stage. CL could be divided into currently and previously formed examples. Currently formed CL underwent remarkable changes in their appearance with the cycle, reflecting ovulation and progesterone production. Thus morphological analysis that is synchronized the large antral follicle changes with recently formed CL ones allows the ovary to be classified into the each estrous cycle stage. Morphological deviation from any synchronized combination provides a first pointer of ovarian toxicity. PCNA immunohistochemical staining is also useful to detect small follicles.

Key words: Estrous cycle, Morphology, Ovarian toxicity, Rat

INTRODUCTION

Detection of ovarian toxicity in preclinical studies is very important for safety assessment of drugs and chemicals, because oocytes have no regenerative ability, and any abnormalities in the ovaries may be directly linked to impairment of female reproductive capacity. The U.S. Environmental Protection Agency (EPA), U.S. Food and Drug Administration (FDA) and the Organization for Economic Cooperation and Development (OECD) recommended qualitative and quantitative evaluation of primordial follicles in the ovary for regulatory guidelines for 2-generation reproductive toxicity studies (U.S. EPA, 1998; U.S. FDA, 2000; OECD, 2001). The ovary has a complicated structure and its appearance changes with the estrous cycle, so that detection of interference with ovarian function requires a comprehensive understanding of the normal variation in ovarian morphology. In particular, the growth of follicles and corpora lutea (CL) and their regression, as well as knowledge on the hypothalmo-pituitary-gonadal axis control system are crucial. Quantitative follicular analysis using serial sections is accepted

Correspondence: Midori Yoshida (E-mail: midoriy@nihs.go.jp)

for assessment of both biological reproduction and toxicology (Bolon *et al.*, 1997; U.S. EPA, 1998; Meredith *et al.*, 1999; OECD, 2001; U.S. FDA, 2000), although the approach is very laborious and time-consuming.

According to the guideline of non-clinical safety studies, the completion of a female fertility study is required prior to the enrollment of women with childbearing potential in phase I clinical trials conducted in Japan. On the other hand, the completion is required prior to phase III clinical trials only in the United States and the European Union. Currently, the ICM M3 program to harmonize these regional differences is progressing (The ICH Steering Committee to the regulatory authorities of the three ICH regions (the European Union, Japan and USA), 2008). For this harmonization, collaboration among the members of the Japan Pharmaceutical Manufacturers Association was organized to conduct validation studies (Sanbuissho *et al.*, 2009). In the validation studies, any improvement to increase attention to toxicity to the female reproductive organs or many conventional guides or references to consistent, reliable and cost-effective methods are required using rat repeated toxicity studies. Recently, immunohistochemical staining of proliferating cell nuclear antigen (PCNA) has been accepted as a useful aid to making ovarian follicle counts, particularly for primordial and primary follicles (Muskhelishvili *et al.*, 2005; Picut *et al.*, 2008). The Society of Toxicologic Pathology (STP) ovary evaluation working group has published a position paper on histopathological approaches for the assessment of rodent reproductive toxicity, and recommended qualitative evaluation of the ovary as the first-tier assessment (Regan *et al.*, 2005). The OECD (2008) is preparing a guidance document for histopathological evaluation with endocrine and reproductive tests to detect chemicals with hormonal potential, including estrogens and antiestrogens. Westwood (2008) has just produced a good practical histological guide of the female reproductive tract in normal cycling rats. However, there is still only limited information on ovarian morphology of relevance to toxicological assessment. The main purpose of the present study was therefore to provide a practical guide of ovarian morphology in rats undergoing normal cycling. In addition, several morphological and methodological points for detection of ovarian toxicity are highlighted.

MATERIALS AND METHODS

Animals

Forty-eight Fischer344 DuCrlCrlj (Fischer) female rats aged 3 months and 92 Crlj:DON (Donryu) female rats aged 3 or 4 months purchased from Charles River Laboratories Japan, Inc. (Kanagawa, Japan) were available for the present study. The animals were maintained in an air-conditioned animal rooms under constant conditions of 24 ± 2°C and 55 ± 10% humidity with a 12-hr light/dark cycle (lighting from 8:00 to 20:00; dark, 20:00 to 8:00), housed 3 or 4 rats per cage, and allowed free access to commercial rodent chow, CRF-1 (Oriental yeast Co., Ltd., Kanagawa, Japan) and drinking water throughout. The Donryu strain rats were checked for estrous cyclicity by vaginal cytology during 9:00-10:00am throughout the study. Animal care and use followed the guidelines for the Care and Use of Laboratory Animals in the National Institute of Health Sciences.

Histology

At necropsy, all animals were euthanized under deep ether anesthesia in the morning. After exsanguination, the ovaries were removed from attached tissues such as ovarian bursa and oviduct, weighed and fixed in 10 vol% neutral buffered formalin. At dissection, the bilateral ovaries were transversally halved to examine maximum areas microscopically. The uterine horn and the vagina also were fixed to allow confirmation of the estrous cycle stage. All of the organs were embedded in paraffin, sectioned at 4 μm and stained with hematoxylin and eosin (HE). All the animals used in the present study showed a normal estrous cycle and the estrous cycle stages at necropsy were determined by vaginal cytology and morphological features in the uterus and the vagina with reference to previous studies (OECD, 2008; Westwood, 2008; Yuan and Foley, 2002).

Immunohistochemistry

Serial sections in the ovaries were incubated with anti-PCNA antibody (Dako Japan, Kyoto, Japan) to find small follicles such as primordial and primary follicles or to distinguish growing follicles as reported by Muskhelishvili *et al.* (2005).

Classification of follicles

In the present study, we applied Pedersen's follicular classification in rodents (Pedersen and Peters, 1968), featuring division into 3 main categories, i.e., small, medium and large corresponding to primordial or primary, preantral, and antral or Graafian follicles, respectively (Table 1). These were further subdivided into 8 types (Types 1 to 8) according to the morphological appearance and follicular size. The classification was established for mouse ovary, but application to the rat or hamster ovary has been recommended (Greenwald and Roy, 1994). In the present

Table 1. Classification of growing follicles

This article	Pedersen and Peters (1968)	Characteristics and Synonyms
Small	Small, Type 1a to 3a	Primordial and primary follicles. Type 3a follicle is a primary follicle with complete ring surrounding small oocyte.
Medium	Medium, Type 3b to 5a	Type 3b follicle is a primary follicle with complete ring surrounding growing oocyte. Secondary follicles and preantral follicles less than 70 μ on the largest cross-section.
Large	Large, Type 5b to 8	Type 5b follicle is preantral one with a fully grown ooctyes surrounded by many layers of granulosa cells. Type 6 follicle is a small antral one with a large oocyte with many layers of granulosa cells and scattered areas of fluid. Type 7 follicle is a antral one with single cavity containing follicle fluid. The cumulus oohorus has formed, but not be formed the stalk. Type 8 follicle is a large antral follicle with a single cavity with follicle fluid and a well-formed cumulus stalk. Type 8 follicle is also termed as Graafian or preovulatory follicles.

study, large follicles without oocytes in the sections were distinguished by morphological features of the granulosa cells and the thickness of the theca cell layer as far as possible. Follicles with apoptotic cells in the granulosa cell layer or degeneration of oocytes were judged as atresia. Atretic follicles were also classified into small, medium or large sized. If necessary, more detailed descriptions based on the follicle size in Pedersen's classification were added.

Classification of CL

CL were divided into currently formed CL and previously formed ones. Currently formed CL, which are also termed as most recently formed or new CL, are defined within one estrous cycle after ovulation. The previously formed CL, which are also termed as old CL, remain in the ovary throughout several estrous cycles before their complete dissolution. In currently formed CL, the ones observed at estrus when ovulation occurred early in the morning were defined as newly formed CL in this article.

Counts of Follicles and newly formed CL

The numbers of each type of follicle, atretic follicles and newly formed CL were counted in unilateral ovaries in F344 rats. Small and medium follicles were recognized on the basis of PCNA positive nuclei. Large follicles and CL were identified primarily in HE-stained samples. Separation was made into each estrous cycle stage. Statistical analysis was with ANOVA and P Values less than 0.05 were considered to be significant.

RESULTS

Small and medium follicles were distributed unevenly throughout the ovary, and they were easily detectable with PCNA immunohistochemical staining (Fig. 1). Small follicles were occasionally aggregated in the cortex. The estrous cycle did not affect their distribution or number. Typical atretic follicles were usually easy to detect at low magnification in HE stained sections. Higher magnification observation after HE staining was often necessary for detection of atretic follicles at early stages, focusing on apoptotic cells in the granulosa cell layer in early stages with other granulosa cells still positive for PCNA (Fig. 2).

Histological characteristics of each estrous cycle stage were as follows:

Proestrus (Fig. 3)

Follicles

Large follicles such as Graafian or Type 8 follicles in Pedersen's classification were evident at this stage. The large follicles Type 8 were located in surface area of the ovary (Figs. 3A-B). Their granulosa cells were cuboidal and/or polygonal, resembling the luteal cells at estrus (Figs. 3C-D). Most large follicles without the cumulus oophorus could be recognized by a thickened theca cell layer or cuboidal or polygonal granulosa cells (Figs. 3E-F). Large follicles Type 7 and some of Type 6 were atretic.

CL

Currently formed CL were starting degenerative processes characterized by vacuoles in cytoplasm, and increased apoptotic cells. Necrosis in the central parts was sometimes observed (Figs. 3G-H). Fibrous tissue proliferation was noted in previously formed CL.

Estrus (Fig. 4)

Follicles

There was a lack of large follicles such as Type 7 or 8. Although distinction of large follicles from degenerated large follicles was sometimes difficult at lower magnification, apoptotic granulosa cells in the degenerated large follicles were recognized them as atretic follicles (Fig. 4C). A number of large follicles of Type 6 were observed.

CL

Newly formed CL were characteristically observed as currently formed ones after ovulation (Figs. 4A-D). They were composed of basophilic, small and spindle-shaped luteal cells, positive for PCNA antibody binding (Figs. 4B-C). In addition, the newly formed CL were easily and clearly distinguishable from the large follicles by angiogenesis between the luteal cells and the break down of the basement membrane between the granulosa cell layer and the theca cell layer (Fig. 4D). Previously formed CL had a similar size as those at proesturs, but degenerative processes including fibrosis were more advanced (Figs. 4E-F).

Metestrus (Fig. 5)

Follicles

There were no large follicles of Type 8, but many large follicles Type 7 were growing (Fig. 5F). Atretic follicles were observed in all types of follicles at a constant rate.

CL

Currently formed CL were characteristically observed. They were increased in size compared to those at estrus, but smaller than those at diestrus (Figs. 5B-D). The luteal cells had still basophilic but not foamy cytoplasm with large nuclei and nucleoli prominent (Fig. 5C). The CL sometimes contained fluid-filled central cavities of various sizes (Figs. 5G-H). PCNA levels in the luteal cells were lower than in that at estrus (Fig. 5I). Previously formed CL demonstrated advanced fibrosis, but their sizes were still similar to those of currently formed examples.

Diestrus (Fig. 6)

Follicles

Large follicles Types 7 and 8 were increased in number, but the latter were smaller than at proestrus (Fig. 6A). Atretic follicles were observed in all types at a constant rate.

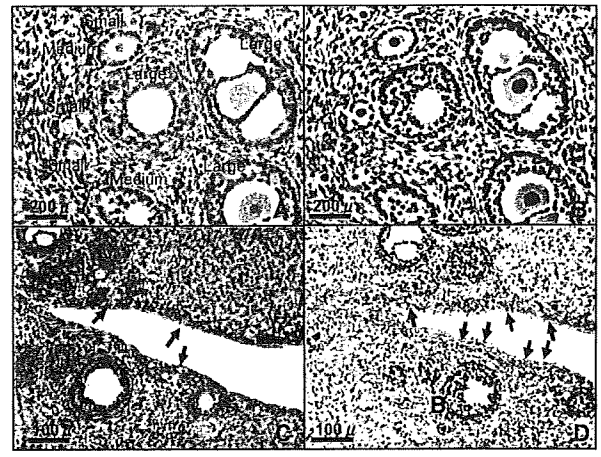

Fig. 1. Classification of follicles. **A**, Small follicles (small), medium follicles (medium), and large follicles are shown. **B**, Immunohistochemical staining for PCNA in a serial section to A. All oocytes and most granulosa cells are positive for PCNA. **C**, Small follicles (arrows) are not distributed uniformly and their identification with HE staining is difficult. **D**, Serial section to C. Note that small follicles (arrows) are easy to detect with PCNA immunohistochemical staining.

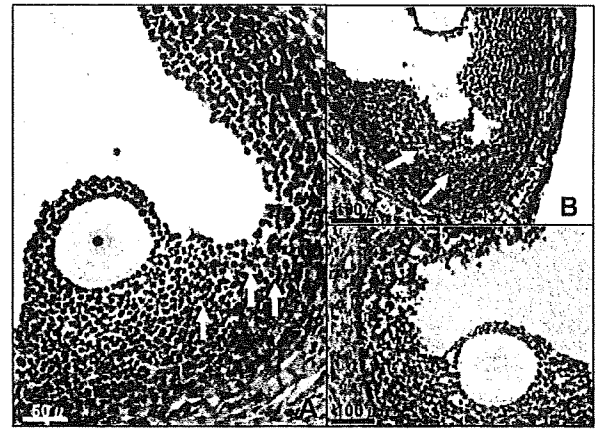

Fig. 2. Various types of atretic follicles. **A**, Early stage. A few apoptotic cells are apparent in the granulosa cell layer in a large follicle (arrows). **B**, Apoptotic cells are scattered in the granulosa cell layer (arrows). **C**, A number of apoptotic cells are present in the lumen and the granulosa cell layer. A-C, HE staining.

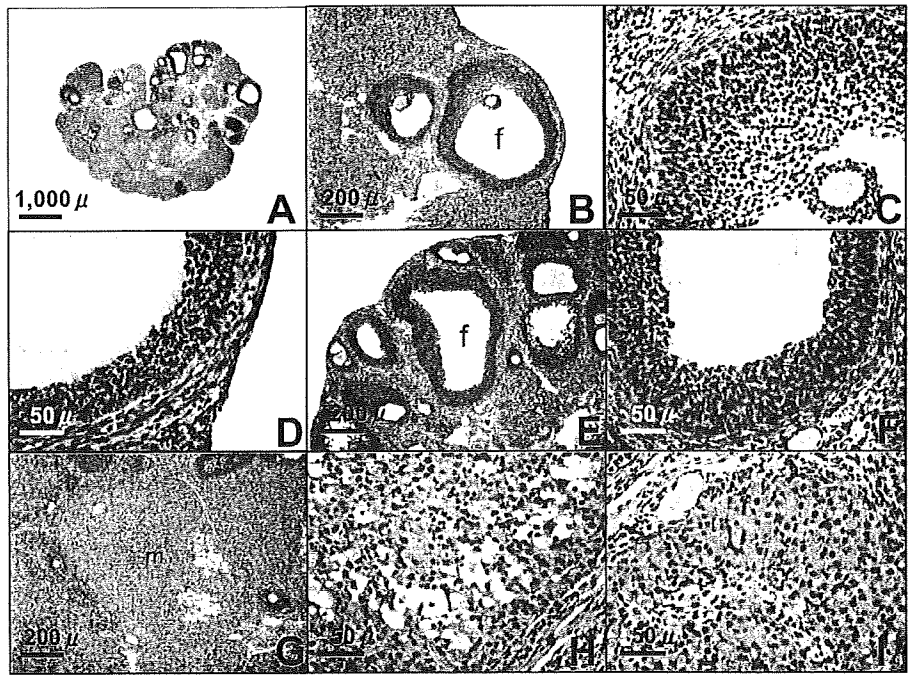

Fig. 3. The ovary at proestrus. **A**, Low-magnification. Large follicles are evident. **B**, A large follicle of Type 8 (f). **C**, Higher magnification of B. Cumulus oophorus formation. **D**, The same large follicle as B. The granulosa cells are round to cuboidal or polygonal in shape, indicating a luteinizing function **E**, A large follicle without cumulus oophorus (f). **F**, Higher magnification of E. Polygonal granulosa cells without apoptotic cells have characteristic of a large follicle Type 8. **G**, A currently formed corpus luteum. **H**, The corpus luteum contains vacuolated, degenerating and necrotic luteal cells in the central portion with some fibrous tissue. **I**, A previously formed corpus luteum. Note proliferation of fibrous tissue. A-I, HE staining.

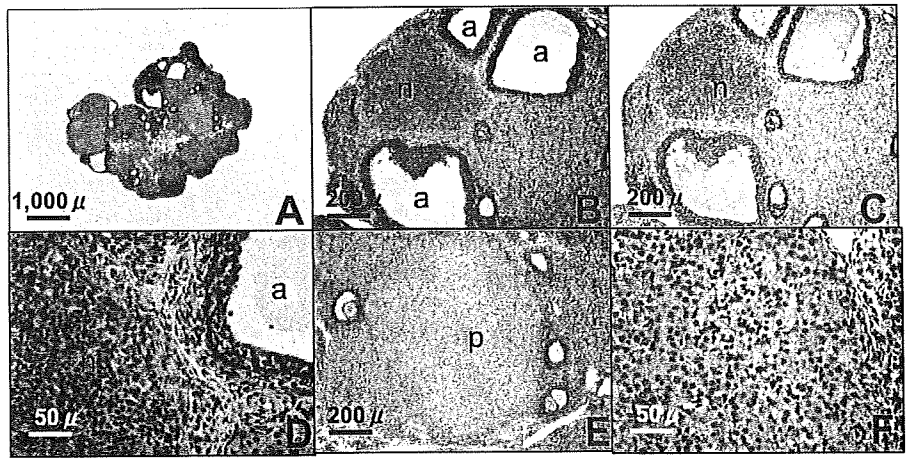

Fig. 4. The ovary at estrus. **A**, Low-magnification. **B**, A currently formed corpus luteum (n) is recognized as a newly formed one at this stage. Large sized atretic follicles are also observed (a). **C**, PCNA immunohistochemical staining of a serial section to B. A newly formed corpus luteum is strongly positive. **D**, Higher magnification of B. Spindle-shaped basophilic luteal cells and capillary formation are observed in a newly formed corpus luteum (n). A large sized atretic follicle is also detected at right upper part (a). **E**, Previously formed corpus luteum (p) of still large size. **F**, Higher magnification of E. Vacuolated and apoptotic cells are apparent. A, B, D-F, HE staining; C, PCNA immunohistochemical staining.

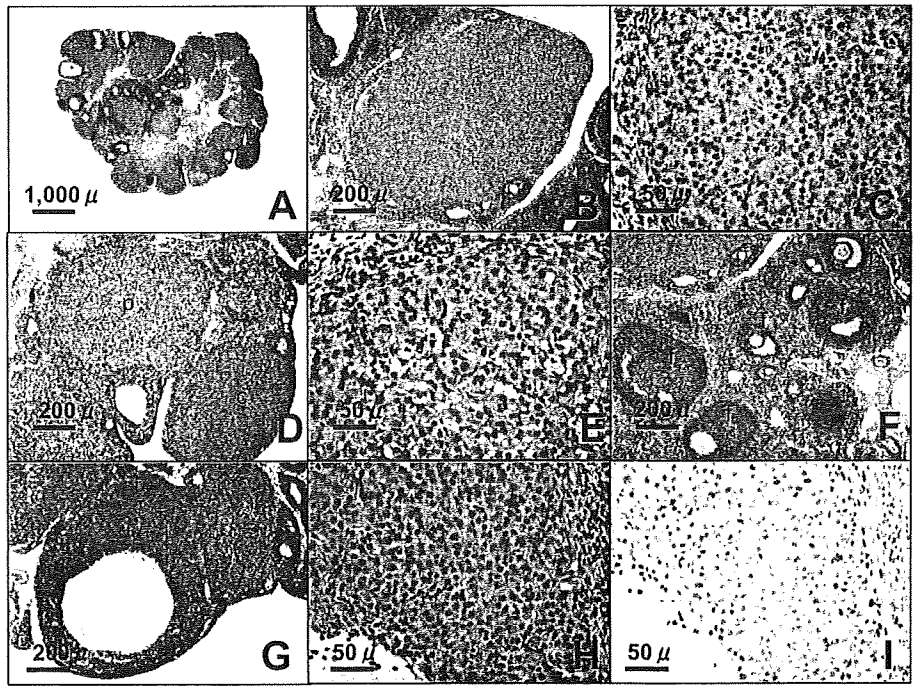

Fig. 5. The ovary at metestrus. **A**, Low-magnification. **B**, A currently formed corpus luteum. **C**, Higher magnification of B. The basophilic luteal cells sometimes exhibit prominent nucleoli. **D**, Currently formed (c) and previously formed (p) CL. Currently formed CL are still smaller than previously formed ones. **E**, A previously formed corpus luteum with fibrous tissue infiltration. **F**, Large follicles of Type 7 (f) appear at this stage. **G**, Currently formed copus luteum with a cavity. **H**, Higher magnification of G. Morphology of the luteal cells is very similar to 5C. **I**, PCNA immunohistochemical staining of a serial section to 5H. A-H, HE staining; I, PCNA immunohistochemical staining.

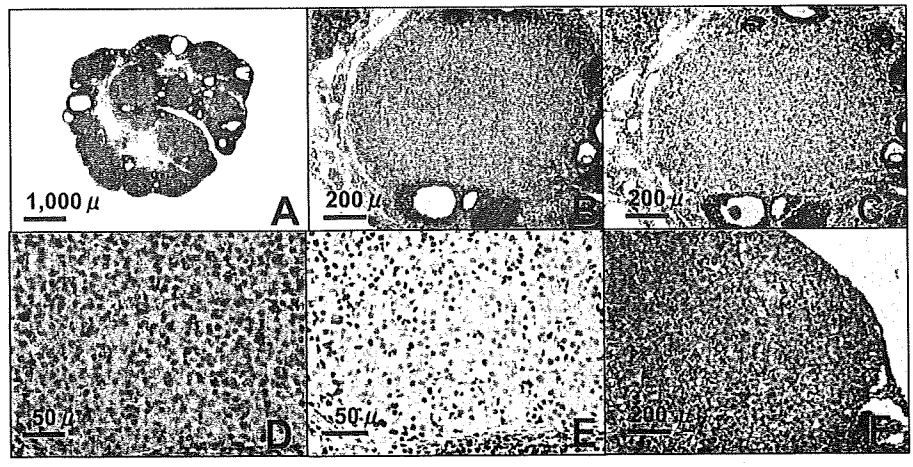

Fig. 6. The ovary at diestrus. **A**, Low-magnification **B**, A currently formed corpus luteum. **C**, A serial section of A immunohistochemically stained with PCNA antibody. **D**, Higher magnification of B. It is larger than at metestrus and the cytoplasm of their component cells is foamy and eosinophilic. **E**, Higher magnification of C. Most luteal cells are negative for PCNA, in contrast to fibrous tissue including fibroblasts or lymphoid cells. **F**, A previously formed corpus luteum with vacuolated luteal cells and fibrous tissue infiltration. A, B, D, F, HE staining. C, E, PCNA immunohistochemical staining.

CL

Currently formed CL had attained the maximum size (Figs. 6A-C). The luteal cells had foamy eosinophilic cytoplasm (Fig. 6D). Most luteal cells were negative for PCNA (Fig. 6E), and fibrous tissue were sometimes detected in the center of CL. Previously formed CL were vacuolated and fibrous tissue infiltration was advanced (Fig. 6F).

The average numbers of follicles and newly formed CL are shown in Table 2. Whereas the numbers of all follicular types and newly formed CL varied, the counts indicated some tendencies as follows: 1) small and medium follicles were found at constant ratios in all stages; 2) large follicles of Type 8 appeared at diestrus and reached a peak in proestrus; and 3) newly formed CL were found only in the estrus stage.

DISCUSSION

The present study demonstrated that the synchronized combination of morphological findings in large follicles, which are follicle stimulating hormone (FSH)-dependent (Greenwald and Roy, 1994), and currently formed CL is allowed as the ovary reliable clarification of each estrous cycle stage. In particular, classification of CL into 2 types appears very useful for staging. There were no morphological differences in either follicles or CLs between F344 and Donryu rats.

Our results for the estrous cycle are similar to those reported previously except for the detailed description of follicular changes (OECD, 2008; Westwood, 2008). In brief, in **proestrus**, the most characteristic feature is the presence of large follicles of Type 8 (Graafian follicles). In addition, cytoplasmic similarity of granulosa cells to luteal cells is characteristic of the Type 8 follicle. The increase in atretic change of Type 7 follicles indicated withdrawal of this type of follicle on the morning after ovulation. While currently formed CL at proestrus resembled those at diestrus, they appeared to be much more regressive. **Estrus** is the easiest stage to recognize due to newly formed CL. Confirmation of angiogenesis in CL in this stage is important to avoid misdiagnosing them from the edge of the Graafian follicles. A lack of large follicles of Types 7 and 8 is also a feature at estrus. Many large follicles of Type 6 might reflect the start of growing large follicles toward next ovulation (Watanabe *et al.*, 1990; Freeman, 2006). **At metestrus**, currently formed CL typicaly had luteal cells with basophilia and prominent nucleoli. This morphology might reflect progesterone production in rats classified into an ultrashort CL species (Freeman, 2006; Stouffer, 2006). **At diestrus,** currently formed CL were still characteristic. They reached the maximum size and contained luteal cells with eosinophilic and foamy cytoplasm. CL are not able to produce active progesterone at this stage (Watanabe *et al.*, 1990; Freeman, 2006).

CLs with cavities were encountered at metestrus in the present study. Their interpretation differs between OECD (2008) and Westwood (2008). Whereas OECD diagnoses them as ovarian luteal cysts which failed ovulation but undergoing luteinization of Graafian follicles in young adult rats (2008), Westwood described them as CL still containing occasional central fluid-filled cavities (2008). In domestic animals, CL with cavities have been accepted not to be confused with cystic follicles or luteinized cysts (Kenndey and Miller, 1993). On the other hand, the distinc-

Table 2. Follicular and newly formed CL counts per unilateral ovary (a) in F344 rats

	Estrous cycle			
Follicle/CL	Proestrus	Estrus	Metestrus	Diestrus
No. of rats examined	13	11	12	12
Follicles				
Small	15.9 ± 2.5 (b)	15.8 ± 3.3	17.0 ± 2.0	20.4 ± 4.4
Medium	2.2 ± 0.5	2.2 ± 0.5	2.0 ± 0.5	2.7 ± 0.4
Large (c)	16.7 ± 1.7	20.9 ± 0.1	18.0 ± 1.4	18.8 ± 2.2
Type 8	2.5 ± 0.3	0	0	0.8 ± 0.3
Atresia	10.8 ± 1.1	8.5 ± 1.4	11.9 ± 1.9	14.5 ± 1.6
CL				
Newly formed	0	1.6 ± 0.4	0	0

(a), the transverse section dissected to obtained maximum cut surface
(b), mean ± S.D.
(c), Including Type 8 follicles

tion between CL with cavity and luteinized cyst is sometimes difficult in rodents, multiovulated species. There are various description of similar morphology showing luteal tissue with cavity, such as CL containing cavities (Westwood, 2008), luteal cyst (OECD, 2008) or cystic CL (Yuan and Foley, 2002). In general, luteinized cysts are easy to distinguish from cystic follicles, which are very large atretic follicles and reflect impair of large follicle growth. They are caused by many chemicals and hormonal disturbances (Bogovich, 1991; Røste *et al.*, 2001; Baravalle *et al.*, 2006). In typical luteinized cyst arising from failure of ovulation and undergoing luteinization, the luteinized cells with angiogenesis formation are found in a thin cell layer or uneven distributed in crescent area in cows (Kenndey and Miller, 1993) and rats (Tamura *et al.*, 2009). The rupture of follicles at ovulation is mainly controlled by progesterone and prostaglandin, and disruptions of these hormones induce unruptured follicles with or without luteinization or formation of luteinized cysts (Davis *et al.*, 1999; Gaytán *et al.*, 2003; Shirota *et al.*, 1998; Tamura *et al.*, 2009; Tsubota *et al.*, 2009; Yuan and Foley, 2002). The CL containing small cavities seems to be normal range in normal cycling rats, because the cavity will be replaced to fibrous tissues next day, at diestrus. However, the toxicological significance of CL with cavities remains to be fully undetermined. We should pay attention an increase of CL containing cavities in treated groups. Further investigation or information is required. Sequential vaginal cytology might be very informative to check ovulation.

Detection of damage to small follicles is very important for detection of ovarian toxicity in preclinical studies. Small follicle counts using single ovarian sections are challenging and evaluation may be misleading (Meredith *et al.*, 1999; Bolon *et al.*, 1997). However, FSH-independent small and medium follicles (Greenwald and Roy, 1994) were observed in all sections examined in the present study and at a constant rate with the estrous cycle stage. The result indicates that lack or only a few visible small follicles in a single ovarian section might give a pointer to alarm for small follicular damage. In addition, PCNA immunohistochemical staining and microscopic observation of bilateral ovaries are helpful to increase the reliability of detection. The STP Ovarian evaluation workshop group (Regan *et al.*, 2005) recommended a qualitative morphological approach for ovarian sections by toxicologic pathologists familiar with normal reproductive cycle as the first tier approach for detection of ovarian toxicity.

In conclusion, the present results demonstrate that ovarian morphology are allowed each estrous cycle stage by combination of morphologic changes in large follicles and CL undergoing development and/or regression (Fig. 7). In the classification of CL into 2 categories, morphological changes in currently formed CL appear particularly useful for staging. In addition, a single ovarian section might be sufficient for analyzing each estrous stage. Our results indicate that any morphological deviation in follicles and CL from the synchronized combination might be the first indicator of ovarian toxicity. PCNA immunohistochemical staining is useful to detect small follicles. Vaginal cytology is also informative for detection of endocrinological condition.

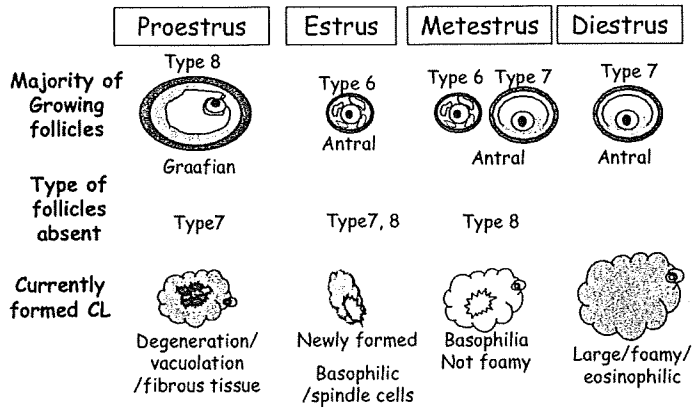

Fig. 7. A scheme for combination of morphologic features in follicles and CL at each estrous cycle in rats. The classification of follicles was referred to Pedersen and Peters (1968).

REFERENCES

Baravalle, C., Salvetti, N.R., Mira, G.A., Pezzone, N. and Ortega, H.H. (2006): Microscopic characterization of follicular structures in letrozole-induced polycystic ovarian syndrome in the rat. Arch. Med. Res., **37**, 830-839.

Bogovich, K. (1991): Induction of ovarian follicular cysts in the pregnant rat by human chorionic gonadotropin. Biol. Reprod., **45**, 34-42.

Bolon, B., Bucci, T.J., Warbritton, A.R., Chen, J.J., Mattison, D.R. and Heindel, J.J. (1997): Differential follicle counts as a screen for chemically induced ovarian toxicity in mice: results from continuous breeding bioassays. Fundam. Appl. Toxicol., **39**, 1-10.

Davis, B.J., Lennard, D.E., Lee, C.A., Tiano, H.F., Morham, S.G., Wetsel, W.C. and Langenbach, R. (1999): Anovulation in cyclooxygenase-2-deficient mice is restored by prostaglandin E2 and interleukin-1beta. Endocrinology, **140**, 2685-95.

Freeman, M.E. (2006): Neuroendocrine control of the ovarian cycle of the rat, In the Physiology of Reproduction, Third Edition (Knobil, E., Neill, J.D. eds.) pp.2327-2388, Raven Press Ltd., New York.

Gaytán, F., Bellido, C., Gaytán, M., Morales, C. and Sánchez-Criado, J.E. (2003): Differential effects of RU486 and indomethacin on follicle rupture during the ovulatory process in the rat. Biol. Reprod., **69**, 99-105.

Greenwald, G.S. and Roy, S.K. (1994): Follicular development and its control. In The Physiology of Reproduction, Second Edition (Knobil, E., Neill, J.D. eds.) pp.629-724, Raven Press Ltd., New York.

Kennedy, P.C. and Miller, R.B. (1993): The female genital system. In Pathology of Domestic Animals. Fourth Edition. (Jubb, K. V. F., Kennedy, P. C., Palmer, N. eds.) pp.349-470, Academic Press, San Diego.

Meredith, S., Dudenhoeffer, G. and Jackson, K. (1999): Single-section counting error when distinguishing between primordial and early primary follicles in sections of rat ovary of different thickness. J. Reprod. Fertil., **117**, 339-343.

Muskhelishvili, L., Wingard, S.K. and Latendresse, J.R. (2005): Proliferating cell nuclear antigen--A marker for ovarian follicle counts. Toxicol. Pathol., **33**, 365-368.

Organization of Economic Cooperation and Development (2001): Proposal for updating Guideline 416: two generation reproduction toxicity study. In OECD Guideline for Testing of Chemicals, pp. 1-13. OECD, Paris.

Organization of Economic Cooperation and Development (OECD) (2008): Draft Guidance and Review Documents/Monographs, Guidance Document for Histopathologic Evaluation of Endocrine and Reproductive Tests. Part 3: Female reproductive system. http://www.oecd.org/document/12/0,3343,en_2649_34377_1898188_1_1_1_1,00.html

Pedersen, T. and Peters, H. (1968): Proposal for a classification of oocytes and follicles in the mouse ovary. J. Reprod. Fertil., **17**, 555-557.

Picut, C.A., Swanson, C.L, Scully, K.L., Roseman, V.C., Parder, R.F. and Remick, A.K. (2008): Ovarian follicle counts using proliferating cell nuclear antigen (PCNA) and semi-automated image analysis in rats. Toxicol. Pathol., **36**, 674-679.

Regan, K.S., Cline, J.M., Creasy, D., Davis, B., Foley, G.L., Lanning, L., Latendresse, J.R., Makris, S., Morton, D., Rehm, S., Stebbins, K. and STP Ovary Evaluation Working Group (2005): STP Position Paper: Ovarian follicular counting in the assessment of rodent reproductive toxicity. Toxicol. Pathol., **33**, 409-412.

Røste, L.S., Taubøll, E., Berner, A., Isojärvi, J.I.T. and Gjerstad, L. (2001): Valproate, but not lamotrigine, induces ovarian morphological changes in Wistar rats. Exp. Toxicol. Pathol., **52**, 545-552.

Sanbuissho, A., Yoshida, M., Hisada, S., Sagami, F., Kudo, S., Kumazawa, T., Ube, M., Komatsu, S. and Ohno, Y. (2009): Collaborative work on evaluation of ovarian toxicity by repeated-dose and fertility studies in female rats. J. Toxicol. Sci., **34** (Special Issue I), SP1-SP22.

Shirota, M., Watanabe, G., Taya, K. and Sasamoto, S. (1998): Effects of indomethacin on the selective release of follicle-stimulating hormone during the period of ovulation in the rat. J. Vet. Med. Sci., **60**, 1059-65.

Smith, B.J., Plowchalk, D.R., Sipes, I.G. and Mattinson, D.R. (1991): Comparison of random and serial sections in assessment of ovarian toxicity. Reprod. Toxicol., **5**, 379-383.

Stouffer, R.L. (2006): Structure, function, and regulation of the corpus luteum. In the Physiology of Reproduction, Third Edition (Knobil, E., Neill, J.D. eds.), pp.475-526. Raven Press Ltd., New York.

Tamura, T., Yokoi, R., Okuhara, Y., Harada, C., Terashima, Y., Hayashi, M., Nagasawa, T., Onozato, T., Kobayashi, K., Kuroda, J. and Kusama, H. (2009): Collaborative work to evaluate ovarian toxicity 2) Two- or four-week repeated dose studies and fertility study of mifepristone in female rats. J. Toxicol. Sci., **34** (Special Issue I), SP31-SP42.

The ICH Steering Committee to the regulatory authorities of the three ICH regions (the European Union, Japan and USA) (2008): Guidance on nonclinical safety studies for the conduct of human clinical trials and marketing authorization for pharmaceuticals. M3(R2). http://www.pmda.go.jp/ich/m/Step3_m3(r2)_08 _07_14_e.pdf

Tsubota, K., Kushima, K., Yamauchi, K., Matsuo, S., Saegusa, T., Ito, S., Fujiwara, M., Matsumoto, M., Nakatsuji, S., Seki, J. and Oishi, Y. (2009): Collaborative work on evaluation of ovarian toxicity 12) Effects of 2- or 4-week repeated dose studies and fertility study of indomethacin in female rats. J. Toxicol. Sci., **34** (Special Issue I), SP129-SP136.

U.S. Environmental Protection Agency (1998): Health Effects Test Guidelines, OPPTS 870.3800, Reproduction and Fertility Effects. EPA 712-C-98-239. U.S. Environmental Protection Agency, Office of Prevention, Pesticides and Toxic Substances, Washington, DC.

U.S. Food and Drug Administration (2000): Redbook 2000. Toxicological Principles for the Safety Assessment for Food Ingredients. IV.C.9.a. Guidelines for Reproductive Studies. U.S. Food and Drug Administration, Center for Food Safety and Applied Nutrition, Washington, DC.

Watanabe, G., Taya, K. and Sasamoto, S. (1990): Dynamics of ovarian inhibin secretion during the oestrous cycle of the rat. J. Endocrinol., **126**, 151-157.

Westwood, F.R. (2008): The female rat reproductive cycle: A practical histological guide to staging. Toxicol. Pathol., **36**, 375-384.

Yuan, Y.D. and Foley, G.L. (2002): Female Reproductive System. In Handbook of Toxicologic Pathology. Second Edition (Haschek, W.M., Rousseaux, C.G., Walling, M.A. eds.), pp.847-894. Academic Press, San-Diego.

Journal of Reproduction and Development, Vol. 55, No. 2, 2009

—Full Paper—

Long-Term Treatment with Bromocriptine Inhibits Endometrial Adenocarcinoma Development in Rats

Midori YOSHIDA[1], Gen WATANABE[2], Tomo SUZUKI[3], Kaoru INOUE[1], Miwa TAKAHASHI[1], Akihiko MAEKAWA[4], Kazuyoshi TAYA[2] and Akiyoshi NISHIKAWA[1]

[1]Division of Pathology, National Institute of Health Sciences, Tokyo 158-8501, [2]Veterinary Physiology, Tokyo University of Agriculture and Technology, Fuchu, Tokyo 183-0054, [3]Pathology Group, Yakult Central Institute, Kunitachi 186-0011 and [4]Safety Assessment Division, Chemical Management Center, National Institute of Technology and Evaluation, Tokyo 151-0066, Japan

Abstract. The effects of long-term blockade of prolactin (PRL) action by bromocriptine (BRC) treatment on uterine carcinogenesis and on related ovarian physiology were investigated using a rat uterine cancer model. Ten-week-old cycling female Donryu rats, a high yield strain for uterine corpus tumors (endometrial adenocarcinomas), were treated with *N-ethyl-N'-nitro-N-nitrosoguanidine* (ENNG), as a tumor initiator, and injected with 1 mg/kg body weight BRC subcutaneously 4 times per week until 14.5 months of age to block the proestrus PRL surge. The study was terminated at 15 months of age, and the results showed that long-term BRC treatment significantly inhibited endometrial adenocarcinoma development in terms of both incidence (34.6% to 13.0% with significant difference at 5%) and multiplicity (0.35 to 0.18 with significant difference at 5%), which indicates the number of adenocarcinomas per animals. While BRC did not affect estrous cyclicity in the treated animals, a significant decline was evident in the serum 17β-estradiol (E2) to progesterone (P) ratio (E: P ratio), and the serum E2 level showed a decreased tendency at 15 months of age. While the precise pathway to the inhibitory effect could not be determined; the pathway by which ovarian hormonal imbalance decreases the serum E: P ratio most likely plays a crucial role.

Key words: Bromocripchne, Long-term treatment, Prolactin blockade, Rat, Uteirne carcinogenesis

(J. Reprod. Dev. 55: 105–109, 2009)

Ovarian steroidhormone imbalance contributes to uterine carcinogenesis in human beings [1]. Maekawa *et al.* [2–4] have provided evidence that a similar imbalance, especially elevated 17β-estradiol (E2) levels relative to progesterone (P) levels (the E:P ratio), plays a crucial role in promoting endometrial adenocarcinoma development in rodents. While it is well-established that E2 and estrogenic chemicals play supportive or sometimes initiative roles in uterine carcinogenesis in rats as well as women, P may exert an inhibitory influence on human uterine cancer development [5–7]. However, the effects of other hormones related to the pituitary or ovaries on uterine carcinogenesis are not well known.

Prolactin (PRL) is one of the important regulators of the corpus luteum as well as luteinizing hormone (LH), prostaglandin and vascular endothelial growth factors and platelet derived growth factors in rats [8–10]. The function of PRL as a luteotrophic and luteolytic hormone, however, is very complex [11–17]. Repeated injection of PRL has been shown to stimulate rapid regression of the persistent corpus luteum, with a concomitant decline in total steroidogenic capacity [12, 18]. These studies indicate the possibility that the modulation of P production induced by PRL or its inhibitor affect uterine carcinogenesis through ovarian hormonal imbalance. On the other hand, PRL receptors, especially long-form ones (PRLR-L) [19], are present in the uteri of rats. PRL is known to play important roles in adenomyosis formation in Swiss mice [20–22]. Bromocriptine (BRC), a dopamine agonist, inhibits inverted growth of the uterine epithelium to the muscle layer in the uterine cervix in ovarietomized mice treated with E2 and PRL [23]. These reports indicate that direct action of PRL on the uterus should be considered as one factor related to uterine carcinogenicity in rats. Blockade of the proestrus PRL surge by treatment with BRC increases the weight of the ovary and the number of corpora lutea in rats without affecting estrous cyclicity [16, 24]. However the long-term effects of BRC treatment on the ovary or uterus have not yet been fully investigated.

In the present study, we therefore focused on the long-term effects of BRC on the ovary and uterine carcinogenesis using the Donryu rat, a high yield strain for endometrial adenocarcinomas.

Accepted for publication: November 6, 2008
Published online in J-STAGE: December 24, 2008
Correspondence: M. Yoshida (e-mail: midoriy@nihs.go.jp)

Materials and Methods

Animals and housing conditions

A total of eighty female Crj:Donryu rats were purchased from Charles River Japan (Yokohama, Japan) at 7–8 weeks of age. The animals were maintained under conditions of controlled temperature (24 ± 2C), humidity (55 ± 10%), and lighting (12-h light/dark cycle). They were housed in plastic cages (3 or 4 animals/cage). Commercial powder diet (CRF-1, Oriental Yeast, Tokyo, Japan) and drinking water were available *ad libitum* throughout the study. Animal care and use were handled in accordance with the guidelines for the care and use of laboratory animals established by the Ethics Committee for Animal Experiments of Sasaki Institute and followed the NIH Guide for the Care and Use of Laboratory

Animals.

Chemicals and selection of the dosing for bromocriptine

BRC (α-ergocryptine; Sigma-Aldrich, St. Lous, MO, USA) was dissolved in DMSO (Wako Pure Chemicals, Osaka, Japan) to produce a dose of 1 mg/kg body weight for subcutaneous administration in 1 ml DMSO/kg body weight. This dose level was selected since it is known to block the proestrus PRL surge [18]. Control animals were administered DMSO only in the same manner.

Impact on uterine carcinogenesis of long-term treatment with BRC

Assessment of the long-term effects of BRC on uterine carcinogenicity was performed using the Donryu rat initiation-promotion assay model for uterine corpus cancer [25]. Briefly, fifty rats at 10 weeks of age were initiated with a single injection of 20 mg/kg *N-ethyl-N'-nitro-N- nitrosoguanidine* (ENNG; Nacalai Tesque, Kyoto, Japan) into one uterine horn via the vagina using a stainless steel catheter. This initiation is known to not be carcinogenetic in organs other than the uterus, and to not affect estrous cyclicity [26]. The animals were allocated into 2 groups, one receiving subcutaneous treatment with BRC five times per week up to 14.5 months of age and the other given DMSO only as the controls. Half a month before termination of the experiment, the treatment was ceased to avoid direct effects of the treatment on the serum hormone profiles. The Donryu strain rat has very regular 4-day estrous cyclicity, and about 60 to 70% of the PRL surge was estimated to be blocked in the treated animals. Clinical signs, body weight changes and estrous cyclicity were checked throughout the study. At 15 months of age, all surviving animals were euthanized by decapitation and necropsied for histopathological assessment and hormone assays as described below. Animals euthanized when moribund or found dead were also examined for histopathology.

Pathology

After complete necropsy of all rats, the ovaries, uteri, adrenals and livers were weighed. These organs and related tissues, including the pituitary, thymus, mammary gland, brain, vagina and sites with macroscopic abnormalities, were fixed in 10% neutral buffered formaldehyde solution and routinely processed for histopathological examination. Both the ovaries were dissected at the maximum transverse sections. In the present study, the upper, middle and lower parts of each uterine horn and the uterine cervix were cut into 3 pieces each in cross-section to detect uterine neoplastic lesions, and the lesions were classified into three degrees of atypical hyperplasia (slight, moderate or severe) and adenocarcinomas, according to the criteria described previously [27]. Atytical hyperplasia was considered to be a precancerous lesion of endometrial adenocarcinoma [27]. Uterine neoplastic lesions were evaluated using the following 2 indicators: the number of animals bearing the most serious neoplastic lesions and the frequency of each neoplastic lesion per animal were expressed as the incidence and multiplicity, respectively.

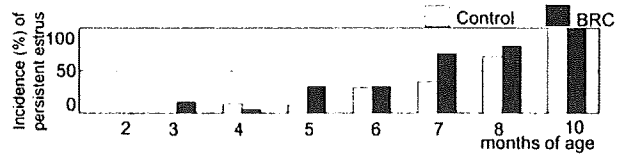

Fig. 1. Incidence of rats showing PE at vaginal cytology until 10 months of age, at which point all animals showed PE. White column (Control): the control group. Black column (BRC) the 1 mg/kg BRC-treated group. No significant differences were detected throughout the treatment.

Radioimmunoassays

Serum samples obtained after decapitation were stored at –80 C until assay. The serum concentrations of follicle-stiumulating hormone (FSH), lutenizing hormone (LH), inhibin, E2, P and PRL were determined using double-antibody radioimmunoassays and ^{125}I-labelled radio-ligands. National Digestive and Kidney Disease (NIDDK) radioimmunoassay kits were employed for rat FSH and LH (NIAMDD, NIH, Bethesda, MD, USA) as described by Taya *et al.* [28] and Watanabe *et al.* [29], respectively. Immunoreactive inhibin in the serum was analyzed using a rabbit anti-serum, TNDH-1[31]. The serum concentrations of E2 and P were also measured as described by Taya *et al.* [29].

Statistical analysis

Incidences values were statistically analyzed using the Fisher's exact probability test. Other data were assessed using t-test (2 groups), and post hoc comparisons between the treated and control groups were made with the Dunnett's *t*-test.

Results

Long-term BRC-treatment did not affect the growth curve or general condition (data not shown). With regard to estrous cyclicity, the vaginal cytology of the BRC-treated group was not different from that of the control group throughout the study. The results were similar to in regard to the occurrences of persistent estrus (PE), abnormal cyclicity including irregular estrous cycle and alterations of cellular components of vaginal smears between the control and BRC-treated groups (Fig. 1). At the end of the study, most of the ovaries were markedly atrophic in both the control and BRC-treated animals (Fig. 2), and no significant differences were detected in the absolute and relative weights of the ovary, uterus, pituitary, liver and spleen between the two groups (Table 1).

Histopathologically, the long-term BRC treatment caused significant reduction in the incidence of endometrial adenocarcinoma and the multiplicity of uterine neoplastic lesions, including both endometrial atypical hyperplasias and adenocarcinomas (Table 2). All adenocarcinomas observed in the control and treated-groups were well-differentiated; poorly- or moderately-differentiated ones were not observed in the BRC-treated animals. The incidence of adenocarinomas was decreased in BRC-treated animals, whereas the incidence of severe atypical endometrial hyperplasia was

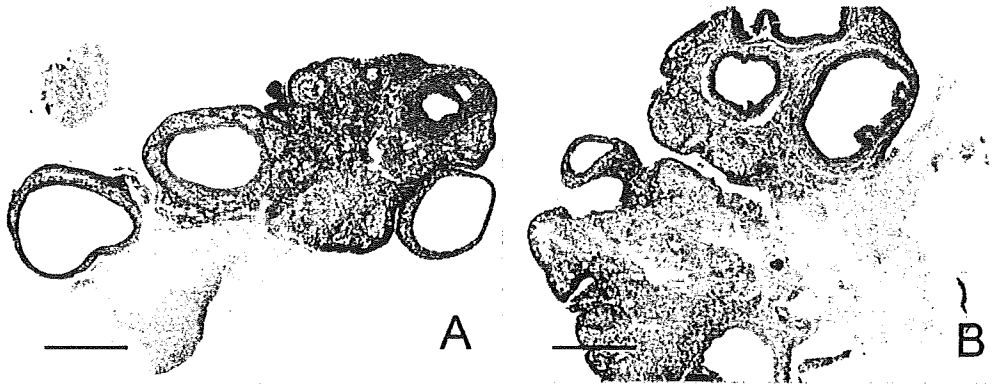

Fig. 2. Histopathology of the ovaries of rats in the control (A) and long-term BRC treatment (B) groups. Both ovaries showed atrophy with cystic atretic follicles and lack of corpora lutea. Bars represent 500 μm. Hematoxylin-eosin staining.

Table 1. Relative organ weights[a] after long-term of treatment with BRC

	Control	BRC-treated
No. of rats at termination	25	23
Pituitary	3.18 ± 2.11[b]	2.14 ± 0.31
Ovaries	12.9 ± 0.72	14.0 ± 0.38
Uterus	325.4 ± 40.1	308.5 ± 16.4
Spleen	173.0 ± 25.1	186.1 ± 14.9
Liver	348.0 ± 48.9	332.1 ± 43.2

[a] Organ weights (mg)/body weight (g) × 100.
[b] Mean ± SD.

increased in this group. The atrophic ovaries of both the BRC-treatment and control groups exhibited similar degrees of cystic or atretic follicles associated with few or no corpora lutea. The occurrences of adenomas and/or adenocarcinomas in the anterior pituitaries or mammary fibroadenomas in the BRC-treated group were comparable to those in the controls. The incidences and intensities of other neoplasms and precancerous lesions were also comparable in the BRC-treated animals and control animals.

At the end of study, the levels of ovarian-derived hormones, such as E2, P and inhibin, at 15 months of age were not significantly different between the BRC-treated and control animals. The E2 levels showed a tendency of decrease in the BRC-treated group (Fig. 3). The ratio of E2 to P was significantly depressed in the BRC-treatment group. The values of pituitary derived hormones, such as PRL, FSH and LH, varied and showed no particular trends.

Discussion

In the present study, long-term BRC treatment significantly inhibited uterine endometrial adenocarcinoma development with regard to both incidence and multiplicity. The incidence of severe atypical endometrial hyperplasia accepted as a precancerous lesion in multi-step tumorigenesis was paradoxically increased, indicating that BRC treatment might inhibit some process in the development of precancerous lesions and step up cancer formation, although the precise mechanism of this was not determined.

Considering the mechanisms underlying the inhibitory effects, decrease of the serum E:P ratio via through ovarian hormonal imbalance most likely plays a crucial role, since the hormonal changes, including the tendency of the serum E2 level to decrease and the significant decrease in the serum E:P ratio, were observed

Table 2. Incidence and multiplicity of uterine neoplastic lesions

Group	No. of rats	None	Hyperplasia			Adenocarcinoma	
			Slight	Moderate	Severe		
Incidence							
Control	26	2	3	7	5	9	
BRC-treated	23	0	2	7	11*	3*	
			Hyperplasia			Adenocarcinoma	Average number of neoplastic lesions
			Slight	Moderate	Severe		
Multiplicity							
Control			0.23 ± 0.51	0.64 ± 0.64	0.38 ± 0.64	0.35 ± 0.49	1.58 ± 0.81
BRC-treated			0.23 ± 0.51	0.17 ± 0.49	0.52 ± 0.59	0.18 ± 0.49*	1.35 ± 0.49

* Significantly different from the control groups ($P<0.05$).